Published in final edited form as:
*Synapse*. 2015 February ; 69(2): 86–95. doi:10.1002/syn.21792.

# Further evaluation of [$^{11}$C]MP-10 as a radiotracer for phosphodiesterase 10A (PDE10A): PET imaging study in rhesus monkeys and brain tissue metabolite analysis

**Shu-fei Lin**, **David Labaree**, **Ming-Kai Chen**, **Daniel Holden**, **Jean-Dominique Gallezot**, **Michael Kapinos**, **Jo-Ku Teng**, **Soheila Najafzadeh**, **Christophe Plisson**, **Eugenii A. Rabiner**, **Roger N. Gunn**, **Richard E. Carson**, and **Yiyun Huang**
PET Center, Department of Diagnostic Radiology, Yale University School of Medicine, New Haven, CT

## Abstract

[$^{11}$C]MP-10 is a potent and specific PET tracer previously shown to be suitable for imaging the PDE10A in baboons with reversible kinetics and high specific binding. However, another report indicated that [$^{11}$C]MP-10 displayed seemingly irreversible kinetics in rhesus monkeys, potentially due to the presence of a radiolabeled metabolite capable of penetrating the blood-brain-barrier (BBB) into the brain. This study was designed to address the discrepancies between the species by re-evaluating [$^{11}$C]MP-10 *in vivo* in rhesus monkey with baseline scans to assess tissue uptake kinetics and self-blocking scans with unlabeled MP-10 to determine binding specificity. *Ex vivo* studies with one rhesus monkey and 4 Sprague-Dawley rats were also performed to investigate the presence of radiolabeled metabolites in the brain. Our results indicated that [$^{11}$C]MP-10 displayed reversible uptake kinetics in rhesus monkeys, albeit slower than in baboons. Administration of unlabeled MP-10 reduced the binding of [$^{11}$C]MP-10 in a dose-dependent manner in all brain regions including the cerebellum. Consequently, the cerebellum appeared not to be a suitable reference tissue in rhesus monkeys. Regional volume of distribution ($V_T$) was mostly reliably derived with the multilinear analysis (MA1) method. In *ex vivo* studies in the monkey and rats only negligible (< 2.7%) amount of radiometabolites was seen in the brain of either species. In summary, results from the present study strongly support the suitability of [$^{11}$C]MP-10 as a radiotracer for PET imaging and quantification of PDE10A in non-human primates.

### Keywords

PET; PDE10A; [$^{11}$C]MP-10; radiometabolite; brain

For correspondence or reprints contact: Shu-fei Lin, Yale PET Center, PO Box 208048, 801 Howard Avenue New Haven, CT 06520. Phone: 203-737-1779; Fax: 203-785-2994.



We have no conflict of interest to declare.

## INTRODUCTION

Cyclic nucleotide phosphodiesterases (PDEs) comprise a group of enzymes with several isoforms that are ubiquitous and important second messengers in the central nervous system, serving to regulate neuronal signal transduction by breaking down either cAMP or cGMP (Soderling and Beavo, 2000). One of these enzymes, PDE10A, has a predominant and selective brain localization in the striatal medium spiny neurons that are the principal site for information integration in the basal ganglia circuitry (Coskran et al., 2006; Soderling et al., 1999), a restricted distribution that appears to be conserved in multiple mammalian species (Coskran et al., 2006). This spatially restricted distribution with high expression and the evidence of altered striatal function in PDE10A knockout mice (Siuciak et al., 2006) suggest that PDE10A may play an important role in striatal signaling. As such, PDE10A is implicated in several neuropsychiatric disorders such as Parkinson's disease, Huntington's disease, schizophrenia, obsessive-compulsive disorder and addiction, and therefore a target for novel drug development aimed at the treatment of these disorders (Menniti et al., 2006).

MP-10, 2-[(4-(1-methyl-4-pyridin-4-yl-1*H*-pyrazol-3-yl)phenoxymethyl]quinoline, is a potent and selective inhibitor of PDE10A (Grauer et al., 2009). It modulates gene expression in both the dopamine $D_1$-direct and $D_2$-indirect striatal pathways and regulates the phosphorylation status of a panel of glutamate receptor subunits in the striatum. We previously reported the evaluation of C-11 labeled MP-10 (Figure 1) in the baboon brain *in vivo*, and demonstrated its suitability as a PET radiotracer with reversible tissue uptake kinetics and high specific binding signals (Plisson et al., 2011). However, in the same year, Tu *et al*. (2011) published their findings in rhesus monkeys that showed seemingly irreversible uptake kinetics of [$^{11}$C]MP-10. This was attributed to the entry of a lipophilic radiolabeled metabolite #1 (Figure 1) into the brain, leading to the steadily increasing uptake of radioactivity in brain tissues throughout the 120 min scan. This species difference in tissue kinetic profiles prompted us to perform a re-evaluation of [$^{11}$C]MP-10 in rhesus monkeys. In addition to PET imaging, *ex vivo* studies were carried out in rats and one rhesus monkey to assess the presence of radiolabeled metabolites in the brain. Herein we reported our findings from these studies.

## MATERIALS AND METHODS

### Chemistry

The radiolabeling precursor for [$^{11}$C]MP-10 and authentic sample of metabolite #1 were gifts from Drs. Zhede Tu and Xiang Zhang of Washington University. Radiosynthesis of [$^{11}$C]MP-10 was carried out according to procedures previously reported through radiolabeling of the pyrazole precursor with [$^{11}$C]methyl iodide (Plisson et al., 2011). Reagents and solvents of appropriate grades for the preparation and analysis of [$^{11}$C]MP-10 were purchased from commercial suppliers and used without further purification.

### Animals

Four rhesus monkeys (*Macaca mulatta*, male, age = 6, 5, 10, and 13 year-old, body weight = 11.6, 7.4, 17, and 11.0 kg, respectively) were included in the PET imaging study. One rhesus

monkey (male, 6.5-year-old, 11.9 kg) and four Sprague–Dawley rats (~ 300 g) were used for *ex vivo* examination of radiolabeled metabolites. Experiments in animals were performed in accordance with protocols approved by the Yale Institutional Animal Care and Use Committee.

### PET Imaging Procedures

Rhesus monkeys were sedated with an intramuscular injection of ketamine hydrochloride (~ 10 mg/kg) ~ 2 h prior to the initiation of PET scans, transported to the PET facility, anesthetized with isoflurane, intubated and maintained on oxygen and 1.5 – 2.5% isoflurane throughout the imaging sessions. PET imaging was performed on the FOCUS-220 PET scanner (Siemens Preclinical Solutions, Knoxville, TN, USA), with an intrinsic image resolution of ~ 1.5 mm. Following a 9-min transmission scan (for attenuation correction), 165 ± 58 MBq (injected mass of 0.016 ± 0.011 μg/kg, n = 8) of radioactivity was administered intravenously over 3 min via an infusion pump (Harvard Apparatus, Holliston, MA, USA). Emission data were acquired in list mode for 120 min and binned into sinograms with 33 successive frames of increasing duration: 6 × 30 s; 3 × 1 min; 2 × 2 min; 22 × 5 min. Dynamic scan data were reconstructed with a FORE/FBP algorithm and a Shepp filter with a cut-off frequency of 0.15 times the sampling frequency (reconstructed image resolution ~ 3.2 mm), with corrections for attenuation, normalization, scatters, and random counts. On each PET scanning day, the animal underwent a baseline scan with [$^{11}$C]MP-10 followed by a blocking scan where a dose of unlabeled MP-10 (0.01, 0.1, 0.3 or 0.6 mg/kg) was administered intravenously 45 min before [$^{11}$C]MP-10 injection.

### Blood Metabolite Analysis, Measurement of Tracer Plasma Free Fraction and Generation of Arterial Plasma Input Function

The arterial plasma input functions corrected for the presence of radiometabolites were generated for all scans based on blood samples taken from the femoral artery. Manual sequential blood samples (0.5–5 mL) were collected at 21 selected time-points during the 120-min scan and plasma was separated from blood cells by centrifugation (2,930 g for 5 min at 4 °C; Allegra X-22R Centrifuge, Beckman Coulter, Fullerton, CA, USA). Whole blood and plasma samples were counted with cross-calibrated gamma well counters (Wizard 1480/ 2480, Perkin Elmer, Waltham, MA, USA).

Plasma samples obtained at 3, 8, 15, 30, 60 and 90 min post-injection were treated with urea (8 M) and then filtered through 1.0 μm Whatman 13 mm GD/X syringe filters (GE, Florham Park, NJ, USA) for metabolite analysis. Up to 5 mL of plasma filtrate was co-injected with unlabeled 4-(1-methyl-4-(pyridin-4-yl)-1H-pyrazol-3-yl)phenol (metabolite #1, Figure 1) and MP-10 onto an automatic column-switching HPLC system (Hilton et al., 2000) equipped with a capture column (19 x 4.6 mm) packed with Phenomenex SPE C18 Strata-X sorbent (Torrance, CA, USA) and eluting with 1% acetonitrile in water at a flow rate of 2 mL/min. After 4 min, activity trapped on the capture column was back-eluted onto a Phenomenex Luna C18(2) analytical column (5 μm, 4.6 x 250 mm) eluting with a mobile phase of 55% acetonitrile and 45% 0.1 M ammonium formate (v/v) at a flow rate of 1.5 mL/min. HPLC eluate was fraction-collected and the fractions were measured with gamma well counters. The sample recovery rate, extraction efficiency, and HPLC fraction recovery were

monitored by measuring radioactivity in the plasma, plasma filter, plasma filtrate, and HPLC fractions. The unmetabolized parent fraction was determined as the ratio of the radioactivity corresponding to the parent (retention time of ~ 11 min) to the total amount of radioactivity collected, fitted with an inverted gamma function. This curve was corrected for the time-varying recovery rate, normalized to the recovery of a reference plasma sample and fitted with an exponential function. The arterial plasma input function was calculated as the product of the plasma time activity curve (TAC) and the parent fraction curve.

Plasma free fraction ($f_p$) was measured with the ultrafiltration method using Millipore Centrifree® micropartition devices (4104, Billerica, MA, USA) following the guidelines provided by the manufacturer with 3 mL of arterial blood taken immediately prior to [$^{11}$C]MP-10 injection and spiked with 7 kBq of [$^{11}$C]MP-10. The free fraction $f_P$ was determined as the radioactivity ratio of ultrafiltrate to plasma.

## Image Processing

Inter-modality registration (PET-to-MRI) was performed using an automated algorithm that chose the optimal transform based on multiple estimates using PET images from different scan periods (Sandiego et al., 2013). Individual MRIs were also warped to a rhesus MRI template using normalized mutual information (NMI) and nonlinear registration (bioimagesuite program; version 2.5; http://www.bioimagesuite.org/) with a modified method of Rueckert *et al*. (Papademetris et al., 2001; Rueckert et al., 1999). The template MRI was created by averaging 8 individual rhesus MRI images that were spatially normalized using a NMI nonlinear registration. Transformation parameters from the individual registrations (template-to-MRI and MRI-to-PET) were combined and applied to the PET dynamic data to derive the time-activity curve (TAC) for each region of interest (ROI). Regional TACs were computed using regions defined on a template brain for the amygdala (0.10 cm$^3$), hippocampus (0.32 cm$^3$), cingulate (0.63 cm$^3$), putamen (0.38 cm$^3$), insula (0.96 cm$^3$), frontal (2.5 cm$^3$), occipital (5.2 cm$^3$), and temporal (3.2 cm$^3$) cortices, globus pallidus (0.13 cm$^3$), caudate (0.43 cm$^3$), nucleus accumbens (0.09 cm$^3$), substantia nigra (0.10 cm$^3$), thalamus (0.25 cm$^3$), cerebellum (5.9 cm$^3$), brainstem (1.9 cm$^3$), and pons (0.33 cm$^3$).

## Tracer Kinetic Analysis

The total volume of distribution ($V_T$) (Innis et al., 2007) was estimated for each ROI. Regional TACs were analyzed with one- (1T) or two-tissue (2T) compartment model (for review, see (Gunn et al., 2001)) and the multilinear analysis-1 (MA1) method (Ichise et al., 2002; Innis et al., 2007) with the plasma TAC as input function. The 1T model is the most simple compartment model, with only two parameters (influx and efflux rate constants), but is often too simplistic to accurately fit PET tracer data. The 2T model is in general sufficient to fit brain TACs, but for some tracer the parameter estimates are too unstable since this model has more (i.e. 4, without blood volume correction) parameters. The MA1 method, which is based on the Logan graphical analysis (Logan et al., 1990), can be suitable for such tracers since it fits brain TACs with any number of underlying compartments (from some time after tracer injection, $t^*$) and only has two parameters.

Receptor occupancy by unlabeled MP-10 was calculated from the occupancy plot using $V_T$ values from all ROIs in the baseline and blocking scans (Cunningham et al., 2010).

### Ex vivo Study in Rhesus Monkey

Under isoflurane anesthesia, one rhesus monkey (male, age = 6.5 year, body weight = 11.9 kg) was administered [$^{11}$C]MP-10 (305 MBq) intravenously. The monkey was euthanized with a lethal dose of pentobarbital 45 min post-injection, after an arterial blood sample was taken. The brain was harvested and dissected. The blood and brain samples were weighed and counted. Blood samples were analyzed using the automatic column-switching HPLC method as described above. Brain samples were first denatured with cold methanol (4 °C, equivalent volumes of tissue samples) and then homogenized with the Kinematica Polytron PT1200 E tissue homogenizer (Luzern, Switzerland). Additional amounts (up to a half the homogenate volume) of saline-methanol mixture (1: 1; v/v) were added to homogenate samples deemed too thick. The homogenates were centrifuged at 4 °C for 10 min at 14,000 rpm with an Eppendorf 5417R benchtop centrifuge (Hauppauge, NY, USA) to precipitate the proteins. Activities in the supernatant and protein pellets were measured and up to 1.0 mL of supernatant was co-injected with solutions of unlabeled metabolite #1 and MP-10 onto the Shimadzu HPLC system (Kyoto, Japan) consisting of a Phenomenex Luna C18(2) analytical column (5 μm, 4.6 × 250 mm), a UV detector (254 nm) and a Flow Cell gamma detector (Gabi Star, Raytest, Straubenhardt, Germany). The column was eluted with a mobile phase of 55% acetonitrile and 45% 0.1M ammonium formate (v/v) at a flow rate of 1.5 mL/min (retention time for [$^{11}$C]MP-10: ~ 8 min; [$^{11}$C]metabolite #1: ~ 3.5 min).

### Ex vivo Study in Sprague–Dawley Rats

[$^{11}$C]MP-10 (30.9 ± 6.3 MBq, n = 4) was administered intravenously via the tail vein to four rats (male, ~ 300 g, Charles River, Richmond, VA). The rats were euthanized with carbon dioxide inhalation at either 30 (n = 2) or 60 min (n = 2) post-injection. Blood samples were collected from the heart and analyzed with the automatic column-switching HPLC method as described above. The brain was dissected into striatum, frontal cortex, hippocampus and cerebellum. Tissue samples were processed and analyzed using the same procedures described above for the rhesus monkey brain samples.

## RESULTS

### Radiochemistry

The radiochemical purity of [$^{11}$C]MP-10 was 98.8 ± 0.8% (n = 9), as determined by analytical HPLC. The specific activity was 963 ± 422 GBq/μmol at the end of synthesis (n = 9).

### PET Imaging Studies in Rhesus Monkeys

**Plasma Analysis—**The radiotracer [$^{11}$C]MP-10 displayed a moderate rate of metabolism in rhesus monkeys (Figure 2A). This rate appeared to be slower than that in baboons, with 56 ± 6% of unmetabolized [$^{11}$C]MP-10 remaining in the plasma of rhesus monkeys at 60 min post-injection (n = 8), compared with 38 ± 6% in baboons (n = 25) (Plisson et al., 2011). No difference in the rate of metabolism was detected between the baseline and

blocking studies (data not shown). The metabolite-corrected plasma TACs from the blocking studies were similar to those from the baseline scans, although the activity in the first 3 min was higher (see Figure 2B for an example) in the blocking studies. [$^{11}$C]MP-10 plasma free fraction ($f_P$) was 0.3 ± 0.1% (n = 8) in monkeys, similar to that in baboons (0.2 ± 0.3%, n = 22).

**Brain Analysis—**An example of baseline [$^{11}$C]MP-10 TACs in monkey brain is shown in Figure 3A. The highest uptake was seen in the putamen, followed by the caudate and frontal cortex, and lower uptake in the occipital cortex and cerebellum, in a pattern similar to that in baboons (Figure 3B) ((Plisson et al., 2011). Regional uptake levels were similar between rhesus monkeys and baboons when expressed in SUV units. The uptake in monkey brain regions plateaued between 70 to 90 min, and then displayed a downward trend in some regions at the end of the 120-min scan. In comparison with baboon TACs, which showed a distinct clearance phase (Plisson et al., 2011), the washout of [$^{11}$C]MP-10 from monkey brain regions appeared to be slower. Faster clearance in baboons may simply be due to more rapid tracer metabolism (Figure 2A).

When the monkeys were treated with increasing doses of unlabeled MP-10, activity concentrations were reduced in a dose-dependent manner in all brain regions, including the high-binding putamen and lowest-binding cerebellum regions (Figure 3C). This suggests the presence of [$^{11}$C]MP-10 specific binding in the cerebellum.

**Tracer Kinetic Analysis—**Baseline [$^{11}$C]MP-10 TACs were analyzed with 1T and 2T compartmental models, as well as the MA1 method using the metabolite-corrected plasma TAC as input function. Visually, the 1T model did not fit ROI TACs well, while the 2T and MA1 provided satisfying fits. Based on the F-test results, the 2T model was better than the 1T model in many regions; however, the 2T model did not provide reliable $V_T$ estimates (i.e., the relative standard error from the covariance matrix was >100%) in many cases (for 69 out of 128 fits). On the other hand, the MA1 method ($t^*$ = 30 min) provided reliable $V_T$ estimates of [$^{11}$C]MP-10 in most ROIs (percent standard error lower than 20% in all regions except for a few fits in a few ROIs, e.g., nucleus accumbens, substantia nigra, and amygdala). The regional $V_T$ values estimated with MA1 from monkeys #1, #2, #3 and #4 are listed in Table I. Monkeys #1 and #3, which were used in the baseline-blocking study with 0.01 or 0.3 mg/kg of unlabeled MP-10, demonstrated much lower SUVs and $V_T$ values in all scans. This substantial inter-animal variation may be attributed to differences in plasma free fraction (see Discussion).

It is interesting to note that, while $V_T$ values for putamen, cingulate cortex, and frontal cortex are similar, the SUV image (Figure 4B) suggests higher uptake in putamen. This difference is due to slower kinetics in the frontal and cingulate cortex regions, so that an SUV image is not completely reflective of the distribution volume, which is the derived equilibrium ratio of tissue to plasma. [$^{11}$C]MP-10 SUV in all brain regions was markedly reduced following pretreatment of the animals with unlabeled MP-10 at a dose of 0.1 or 0.6 mg/kg (Figures 4C and 4D).

Assuming that the endogenous PDE10A occupancy is negligible at baseline and PDE10A occupancy is the same across all regions after administration of the PDE10A inhibitor (i.e. MP-10 in this study), occupancy by MP-10 was estimated from the slope of the occupancy plot regression lines (Cunningham et al., 2010) (see Figure 5 for an example plot). These occupancy estimates were 50.5, 91.5, 98.6 and 98.7 %, respectively, for the 0.01, 0.1, 0.3 and 0.6 mg/kg MP-10 blocking doses, which are highly consistent with the range of doses applied. The non-displaceable volume of distribution ($V_{ND}$) was also estimated from the occupancy plots, as the x-intercept of the regression line (Figure 5). [$^{11}$C]MP-10 $V_{ND}$ was estimated to be 0.4, 2.2, 0.6, and 2.0 mL/cm$^3$ for monkeys #1 to #4, respectively (with inter-animal variation potentially due to differences in plasma free fraction). Based on the derived $V_{ND}$ values for individual animals, [$^{11}$C]MP-10 binding potential ($BP_{ND}$) values, calculated as $BP_{ND} = (V_{T\ ROI} - V_{ND}) / V_{ND}$, were estimated at 4.5 to 10.1 in the putamen, 3.8 to 8.9 in the caudate and 2.0 to 4.3 in the cerebellum in the baseline scans (Table I). Thus, the inter-animal variation in $BP_{ND}$ was smaller than that in absolute $V_T$ values.

**Metabolite Analysis—**Analysis of radioactive metabolites was carried out with plasma and brain samples from monkeys and rats. All radiometabolites appeared to be more polar than the parent compound [$^{11}$C]MP-10. Figure 6 presents HPLC chromatograms from plasma samples taken at 60 min post-injection of [$^{11}$C]MP-10 in rats and monkeys (this study), and baboons (Plisson et al., 2011), while Figure 7 shows the analysis results from rat and monkey brain regions. Metabolite #1 (retention time of 7.5 min, Figure 1), identified by Tu *et al*. as the dealkylated product of [$^{11}$C]MP-10, appeared in the plasma of all three species, in addition to some polar radioactive metabolites not retained on the capture column during the first 4 min in our column-switching analytical HPLC system (Figure 6). At 60 min post-injection, the highest amount of metabolite #1 in the plasma was observed in the rat (38.5 ± 11.5%, n = 2), followed by that in the baboon (27.6 ± 9.0%, n = 25), and the lowest in the monkey (9.9 ± 3.6%, n = 4) (Tables II & III). The percentage of polar metabolites was about the same at 60 min post-injection among the three species.

In the analysis of monkey striatum and cerebellum samples taken at 45 min following [$^{11}$C]MP-10 injection, no radiometabolites in the supernatant of tissue extracts were observed on the HPLC gamma chromatograms (Figure 7). Results based on gamma counts of HPLC eluent fractions are presented in Table II and demonstrate the presence of negligible amount of radiometabolites in the monkey brain (< 2.5%), whereas radiometabolites accounted for 27.7% of the total radioactivity in the plasma (Table II).

Similarly, in the analysis of rat striatum and mixture of frontal cortex, hippocampus and cerebellum taken at 30 or 60 min following [$^{11}$C]MP-10 injection, no peaks for any radioactive metabolites were visible on the gamma HPLC chromatograms (Figure 7), and gamma counts of HPLC eluent fractions detected only negligible amount of radiometabolites at 30 min post-injection and a small amount of metabolite #1 (Figure 1) at 60 min post-injection (6.0% in the brain mixture) (Table III). These results were in sharp contrast to those from analysis of plasma samples, where radiometabolites accounted for ~ 48% and 68% of the total activity at 30 and 60 min post-injection, respectively.

## DISCUSSION

[$^{11}$C]MP-10 has been demonstrated to be a suitable PET radiotracer in baboons for imaging PDE10A, with reversible tissue kinetics and high specific binding signals (Plisson et al., 2011). However, seemingly irreversible uptake kinetics for [$^{11}$C]MP-10 was reported by Tu *et al*. in rhesus monkeys, purportedly due to the entry of a radioactive metabolite (metabolite #1, Figure 1) into the monkey brain (Tu et al., 2011). To address the discrepancy between the species, we carried out a reevaluation of [$^{11}$C]MP-10 with PET imaging study in rhesus monkeys and *ex vivo* analysis in a rhesus monkey and Sprague-Dawley rats. Results from the present study indicated that [$^{11}$C]MP-10 had slower uptake kinetics in monkeys than baboons, a result that may be attributable in part to the slower peripheral metabolism and clearance of [$^{11}$C]MP-10 in monkeys. In the monkey brain, [$^{11}$C]MP-10 displayed a regional uptake pattern in accordance with the regional concentrations of PDE10A in the primates (Coskran et al., 2006). Despite its slower kinetics and high inter-animal variability of brain uptake in monkeys, we did not observe the upward trend in [$^{11}$C]MP-10 brain uptake reported by Tu *et al*.2011. Instead, our results showed that activity in the monkey brain plateaued between 70–90 min in most regions and an appreciable clearance was observed in some regions at the end of the 120-min scan. There appeared to be no major differences in the size and gender of monkeys used between the studies of ours and Tu *et al.* (2011). At present time, it is not clear what caused such a discrepancy in [$^{11}$C]MP-10 uptake kinetics in rhesus monkeys between the two groups.

Regional TACs of [$^{11}$C]MP-10 in the monkey brain were well fitted with kinetic models and regional $V_T$ values were most reliably derived with the MA1 method in comparison with other models. In addition, pretreatment with unlabeled MP-10 reduced $V_T$ in all brain regions in a dose dependent manner, thus our results demonstrated the binding specificity of [$^{11}$C]MP-10 in the rhesus monkey brain. Reduction of $V_T$ values in low binding regions such as the cerebellum suggests the presence of [$^{11}$C]MP-10 specific binding, consistent with results from immunohistochemical staining in cynomolgus monkey indicating the existence of PDE10A immunoreactivity in the neuronal nuclei of cerebellum (Coskran et al., 2006). It also indicates the lack of a reference region for [$^{11}$C]MP-10 in rhesus monkeys. However, the cerebellum has been suggested as a good reference tissue for the assessment of regional binding potentials for [$^{11}$C]MP-10 in baboons (Plisson et al., 2011) and for two structurally related PDE10 tracers [$^{18}$F]MNI654 and [$^{18}$F]MNI659 in rhesus monkeys, baboons (Barret et al., 2012; Barret et al., 2014) and humans (Jennings 2013), and for [$^{11}$C]Lu AE92686 in cynomolgus monkeys (Kehler et al., 2014). In another study, the frontal cortex was used as the reference region in the human brain for [$^{18}$F]JNJ42259152, a structural analogue of [$^{11}$C]MP-10 (Van Laere et al., 2013). In addition, the cerebellum and thalamus have been considered as alternative reference regions. In yet another study with the novel PDE10 tracer [$^{11}$C]AMG 7980 in baboons, thalamus was used as a reference region, even though a difference in the thalamic $V_T$ and $V_{ND}$ derived from blocking experiments was indicated (Hwang et al., 2014). Apparently, an optimal reference region for PDE10 tracers in either non-human primates or humans is far from settled, and further studies are needed to clarify this situation.

Using the non-specific volume of distribution ($V_{ND}$) estimated from the blocking studies, regional $BP_{ND}$ values were calculated for [$^{11}$C]MP-10 baseline scans in the brain of individual monkeys. Regional $BP_{ND}$ values ranged from 4.5 to 10.1 in the putamen, 3.8 to 8.9 in the caudate and 2.0 to 4.3 in the cerebellum (n = 4), another indication that [$^{11}$C]MP-10 can provide good specific binding signals in regions of the rhesus monkey brain. Note that the dose of MP-10 to achieve 50% occupancy, $ED_{50}$, is quite different in baboons and rhesus monkeys: ~ 0.01 mg/kg in monkeys vs. ~ 0.3 mg/kg in baboons as derived from the blocking studies (Plisson et al., 2011). This indicates that the affinity of MP-10 is likely to be substantially higher in rhesus than baboon, another factor that may contribute to the slower kinetics of [$^{11}$C]MP-10 in rhesus monkeys.

We found substantial inter-animal variability in regional $V_T$ values (Table I). Although we cannot absolutely reconcile this result, one potential explanation is inter-animal variation in plasma free fraction ($f_P$). Free fraction should affect the absolute values of $V_T$ and may also affect the tracer delivery rate ($K_1$) (Innis et al., 2007). In the 4 rhesus monkeys used here, the animals with higher values of $V_T$ also had higher values of $K_1$, based on 1T or 2T model fitting (data not shown). Ideally, $f_P$ could be measured and used to correct the $V_T$ data, as we have done successfully in a previous nonhuman primate study (Gallezot et al., 2011). However, due to the very low measured $f_P$ values of [$^{11}$C]MP-10, they are not considered to be accurate, as they can be affected by small quantities of radiochemical impurities. Note also that inter-animal variation in $V_T$ was not seen in our previous study (Plisson et al., 2011), however, the baboons in that study all had very similar ages and weights, unlike in the current study. Thus, larger inter-animal variation in $f_P$ in the current study is highly possible.

The second primary aim of the present study was to verify if any radiolabeled metabolites from [$^{11}$C]MP-10 penetrated the BBB and contributed to the continuing rise in radioactivity uptake in the monkey brain observed by Tu *et al*. (Tu et al., 2011). Their reported TACs showed an irreversible uptake, with SUVs increasing continuously from ~ 1 at the beginning to >3 in the cerebellum and ~5 in the striatum at the end of the 120-min scan. Such dramatic increase in brain uptake was attributed to the presence of radiolabeled metabolite #1 (Figure 1) in the monkey brain. However, in our current *ex vivo* study in a rhesus monkey, no presence of radiometabolite #1 was observed in either the striatum or cerebellum at 45 min post-injection of [$^{11}$C]MP-10. Hence, we believe that the regional uptake of [$^{11}$C]MP-10 in our present study reflects the authentic distribution of the parent radiotracer in the rhesus monkey brain, a fact reinforced by the similarity in uptake kinetics and distribution pattern shown here and those from baboons (Plisson et al., 2011).

The assumption by Tu *et al*. (2011) of radioactive metabolite #1 penetrating into the monkey brain was based on the analysis of rat whole brain samples. In an effort to verify their findings, we also conducted *ex vivo* analysis of radioactivity in the rat brain regions. Even though the presence of radiometabolites in the rat brain was not clearly visible on the gamma HPLC chromatograms, we did observe from our counting results a small amount of radiolabeled metabolite #1 in the brain mixture of cerebellum, frontal cortex and hippocampus (6.0%) at 60 min after [$^{11}$C]MP-10 injection. However, this percentage was much lower than that observed by Tu *et al*. (~ 16% of radiometabolite #1 present in the

brain at the same time point). This difference could be due to the heterogeneous distribution of radiometabolite #1, resulting in some brain regions containing more than the others. Tu *et al*. (2011) examined the whole brain, while we dissected the striatum, frontal cortex, hippocampus, and cerebellum for analysis.

The major difference in chromatographic behavior of [$^{11}$C]MP-10 and its metabolites in plasma samples between our laboratory and that of Tu *et al*. (2011) was a group of extremely polar metabolites. This group of "polar metabolites" was poorly retained on the short capture column packed with C18 material and eluted out during the enrichment process when 1% acetonitrile in water was used as the mobile phase. They were well separated from metabolite #1, which was eluted off the analytical column at ~3.5 min after the mobile phase was switched (Figure 6). In the report of Tu *et al*. (2011), metabolite #1 was eluted off the column at ~3 min, apparently very close to the solvent front. As a result, the radioactive peak labeled "metabolite #1" may not be just a single compound, but rather a combination of the identified metabolite #1 and other polar radioactive species. These differences in chromatographic conditions may well contribute to differences in the accounting of "metabolite #1" between our two groups in the analysis of plasma samples.

In summary, re-evaluation of the radiotracer [$^{11}$C]MP-10 in rhesus monkeys confirmed our previous findings in baboons: that it presented good brain uptake, reversible tissue kinetics, PDE10A binding specificity and high specific binding signal. Further, we demonstrated that [$^{11}$C]MP-10 binding parameters can be reliably derived with kinetic modeling using the MA1 method. Different [$^{11}$C]MP-10 metabolism rates were observed among the species: faster in rats and slower in monkeys, with baboons in between. However, we failed to replicate the observation of Tu *et al*. (2011) that [$^{11}$C]MP-10 displayed irreversible tissue binding characteristics in rhesus monkeys. In addition, we showed that there was no appreciable amount of radioactive metabolites in the brain of rhesus monkey and thus overturned the assumption of a radioactive metabolite entering the monkey brain. Taken together, results from the present study confirm that [$^{11}$C]MP-10 is a potent and specific radioligand suitable for PET imaging and quantification of PDE10A binding sites in the non-human primate brain and hence further evaluation of [$^{11}$C]MP-10 in humans is warranted.

## CONCLUSION

PET scans with [$^{11}$C]MP-10 in rhesus monkeys demonstrated tissue kinetics and specific binding signals consistent with our previous observations in baboons. Little or no radioactive metabolites were found in the brain of monkey, or rat. Hence, our results strongly support the suitability of [$^{11}$C]MP-10 for PET imaging and quantification of PDE10A.

## Acknowledgments

We gratefully acknowledge the expert technical assistance from the staff of the Yale PET Center. This publication was also made possible by CTSA Grant Number UL1 RR024139 from the National Center for Research Resources (NCRR) and the National Center for Advancing Translational Science (NCATS), components of the National Institutes of Health (NIH), and NIH roadmap for Medical Research.

## References


Barret O, Thomae D, Alagille D, Lee H, Papin C, Baldwin R, Jennings D, Marek K, Seibyl J, Tamagnan G. First in vivo assessment of two PDE10 tracers $^{18}$F-MNI654 and $^{18}$F-MNI659. J Nucl Med. 2012; 53(1):361.

Barret O, Thomae D, Tavares A, Alagille D, Papin C, Waterhouse R, McCarthy T, Jennings D, Marek K, Russell D, Seibyl J, Tamagnan G. *In vivo* assessment and dosimetry of 2 novel PDE10A PET radiotracers in humans: $^{18}$F-MNI-659 and $^{18}$F-MNI-654. J Nucl Med. 2014; 55(8):1297–1304. [PubMed: 24898025]

Coskran TM, Morton D, Menniti FS, Adamowicz WO, Kleiman RJ, Ryan AM, Strick CA, Schmidt CJ, Stephenson DT. Immunohistochemical localization of phosphodiesterase 10A in multiple mammalian species. J Histochem Cytochem. 2006; 54(11):1205–1213. [PubMed: 16864896]

Cunningham VJ, Rabiner EA, Slifstein M, Laruelle M, Gunn RN. Measuring drug occupancy in the absence of a reference region: the Lassen plot re-visited. J Cereb Blood Flow Metab. 2010; 30(1): 46–50. [PubMed: 19738632]

Gallezot JD, Weinzimmer D, Nabulsi N, Lin SF, Fowles K, Sandiego C, McCarthy TJ, Maguire RP, Carson RE, Ding YS. Evaluation of [$^{11}$C]MRB for assessment of occupancy of norepinephrine transporters: Studies with atomoxetine in non-human primates. Neuroimage. 2011; 56(1):268–279. [PubMed: 20869448]

Grauer SM, Pulito VL, Navarra RL, Kelly MP, Kelley C, Graf R, Langen B, Logue S, Brennan J, Jiang L, Charych E, Egerland U, Liu F, Marquis KL, Malamas M, Hage T, Comery TA, Brandon NJ. Phosphodiesterase 10A inhibitor activity in preclinical models of the positive, cognitive, and negative symptoms of schizophrenia. J Pharmacol Exp Ther. 2009; 331(2):574–590. [PubMed: 19661377]

Gunn RN, Gunn SR, Cunningham VJ. Positron emission tomography compartmental models. J Cereb Blood Flow Metab. 2001; 21(6):635–652. [PubMed: 11488533]

Hilton J, Yokoi F, Dannals RF, Ravert HT, Szabo Z, Wong DF. Column-switching HPLC for the analysis of plasma in PET imaging studies. Nucl Med Biol. 2000; 27(6):627–630. [PubMed: 11056380]

Hwang DR, Hu E, Rumfelt S, Easwaramoorthy B, Castrillon J, Davis C, Allen JR, Chen H, Treanor J, Abi-Dargham A, Slifstein M. Initial characterization of a PDE10A selective positron emission tomography tracer [$^{11}$C]AMG 7980 in non-human primates. Nucl Med Biol. 2014; 41(4):343–349. [PubMed: 24607437]

Ichise M, Toyama H, Innis RB, Carson RE. Strategies to improve neuroreceptor parameter estimation by linear regression analysis. J Cereb Blood Flow Metab. 2002; 22(10):1271–1281. [PubMed: 12368666]

Innis RB, Cunningham VJ, Delforge J, Fujita M, Gjedde A, Gunn RN, Holden J, Houle S, Huang SC, Ichise M, Iida H, Ito H, Kimura Y, Koeppe RA, Knudsen GM, Knuuti J, Lammertsma AA, Laruelle M, Logan J, Maguire RP, Mintun MA, Morris ED, Parsey R, Price JC, Slifstein M, Sossi V, Suhara T, Votaw JR, Wong DF, Carson RE. Consensus nomenclature for in vivo imaging of reversibly binding radioligands. J Cereb Blood Flow Metab. 2007; 27(9):1533–1539. [PubMed: 17519979]

Jennings D, Papapetropoulos S, Rikki WN, Barret O, Friedman JH, Russell D, Tamagnan G. Examining expression of phosphodiesterase 10A (PDE10A) in Huntington's disease using $^{18}$F-MNI-659 PET. Mov Disord. 2013; 28 (1):161. [PubMed: 23239285]

Kehler J, Kilburn JP, Estrada S, Christensen SR, Wall A, Thibblin A, Lubberink M, Bundgaard C, Brennum LT, Steiniger-Brach B, Christoffersen CT, Timmermann S, Kreilgaard M, Antoni G, Bang-Andersen B, Nielsen J. Discovery and development of $^{11}$C-Lu AE92686 as a radioligand for PET imaging of phosphodiesterase10A in the brain. J Nucl Med. 2014; 55(9):1513–8. [PubMed: 24994928]

Logan J, Fowler JS, Volkow ND, Wolf AP, Dewey SL, Schlyer DJ, MacGregor RR, Hitzemann R, Bendriem B, Gatley SJ, et al. Graphical analysis of reversible radioligand binding from time-activity measurements applied to [*N*-$^{11}$C-methyl]-(−)cocaine PET studies in human subjects. J Cereb Blood Flow Metab. 1990; 10(5):740–747. [PubMed: 2384545]

Menniti FS, Faraci WS, Schmidt CJ. Phosphodiesterases in the CNS: targets for drug development. Nat Rev Drug Discov. 2006; 5(8):660–670. [PubMed: 16883304]

Papademetris X, Jackowski AP, Schultz RT, Staib LH, Duncan JS. Integrated Intensity and Point-Feature Nonrigid Registration. Med Image Comput Comput Assist Interv. 2001; 3216(2004):763–770. [PubMed: 20473359]

Plisson C, Salinas C, Weinzimmer D, Labaree D, Lin SF, Ding YS, Jakobsen S, Smith PW, Eiji K, Carson RE, Gunn RN, Rabiner EA. Radiosynthesis and in vivo evaluation of [$^{11}$C]MP-10 as a positron emission tomography radioligand for phosphodiesterase 10A. Nucl Med Biol. 2011; 38(6):875–884. [PubMed: 21843784]

Rueckert D, Sonoda LI, Hayes C, Hill DLG, Leach MO, Hawkes DJ. Nonrigid registration using free-form deformations: application to breast MR images. Medical Imaging, IEEE Trans Med Imaging. 1999; 18(8):712–721.

Sandiego CM, Weinzimmer D, Carson RE. Optimization of PET-MR registrations for nonhuman primates using mutual information measures: a Multi-Transform Method (MTM). Neuroimage. 2013; 64:571–581. [PubMed: 22926293]

Siuciak JA, McCarthy SA, Chapin DS, Fujiwara RA, James LC, Williams RD, Stock JL, McNeish JD, Strick CA, Menniti FS, Schmidt CJ. Genetic deletion of the striatum-enriched phosphodiesterase PDE10A: evidence for altered striatal function. Neuropharmacol. 2006; 51(2):374–385.

Soderling SH, Bayuga SJ, Beavo JA. Isolation and characterization of a dual-substrate phosphodiesterase gene family: PDE10A. Proc Natl Acad Sci U S A. 1999; 96(12):7071–7076. [PubMed: 10359840]

Soderling SH, Beavo JA. Regulation of cAMP and cGMP signaling: new phosphodiesterases and new functions. Curr Opin Cell Biol. 2000; 12(2):174–179. [PubMed: 10712916]

Tu Z, Fan J, Li S, Jones LA, Cui J, Padakanti PK, Xu J, Zeng D, Shoghi KI, Perlmutter JS, Mach RH. Radiosynthesis and in vivo evaluation of [$^{11}$C]MP-10 as a PET probe for imaging PDE10A in rodent and non-human primate brain. Bioorg Med Chem. 2011; 19(5):1666–1673. [PubMed: 21315609]

Van Laere K, Ahmad RU, Hudyana H, Dubois K, Schmidt ME, Celen S, Bormans G, Koole M. Quantification of $^{18}$F-JNJ-42259152, a novel phosphodiesterase 10A PET tracer: kinetic modeling and test-retest study in human brain. J Nucl Med. 2013; 54(8):1285–1293. [PubMed: 23843566]

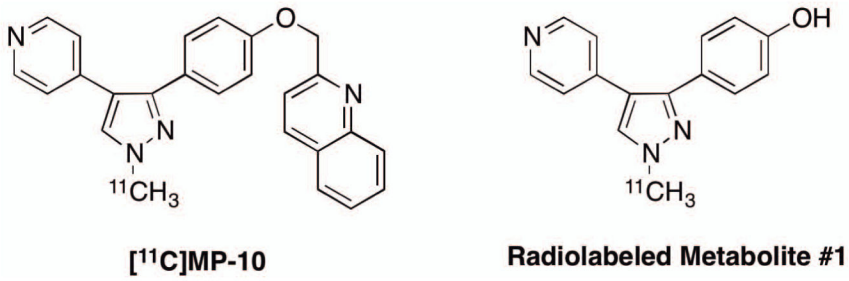


**Figure 1.**
Structures of [$^{11}$C]MP-10 and one of its radiometabolites.

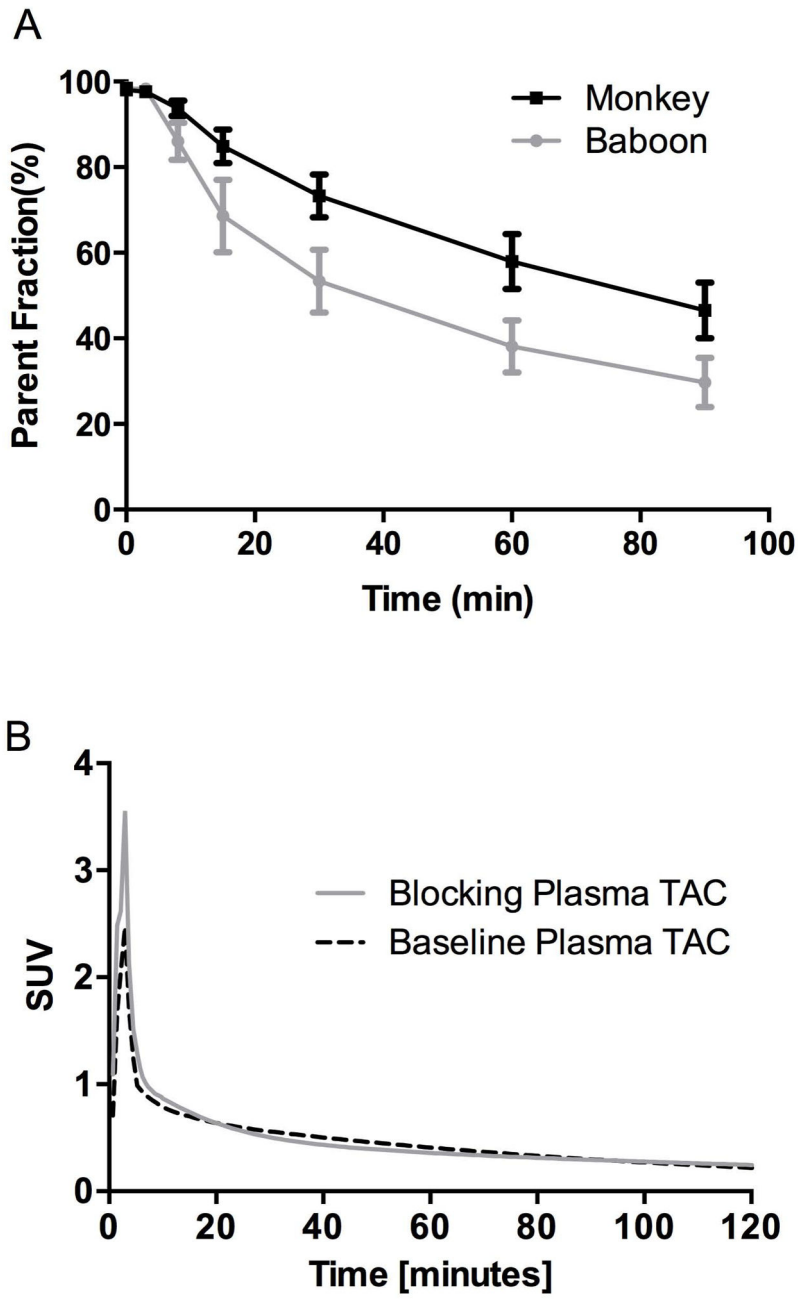


**Figure 2.**

A. [$^{11}$C]MP-10 parent fractions in the plasmas of rhesus monkeys and baboons. The error bars represent the standard deviation (n = 8 for monkey; n = 25 for baboon). B. [$^{11}$C]MP-10 metabolite-corrected arterial plasma TACs in a rhesus monkey from the blocking study (0.6 mg/kg) with unlabeled MP-10 and its corresponding baseline scan. Radioactivity concentrations are expressed in SUV units (concentration / (injected dose/body weight)).

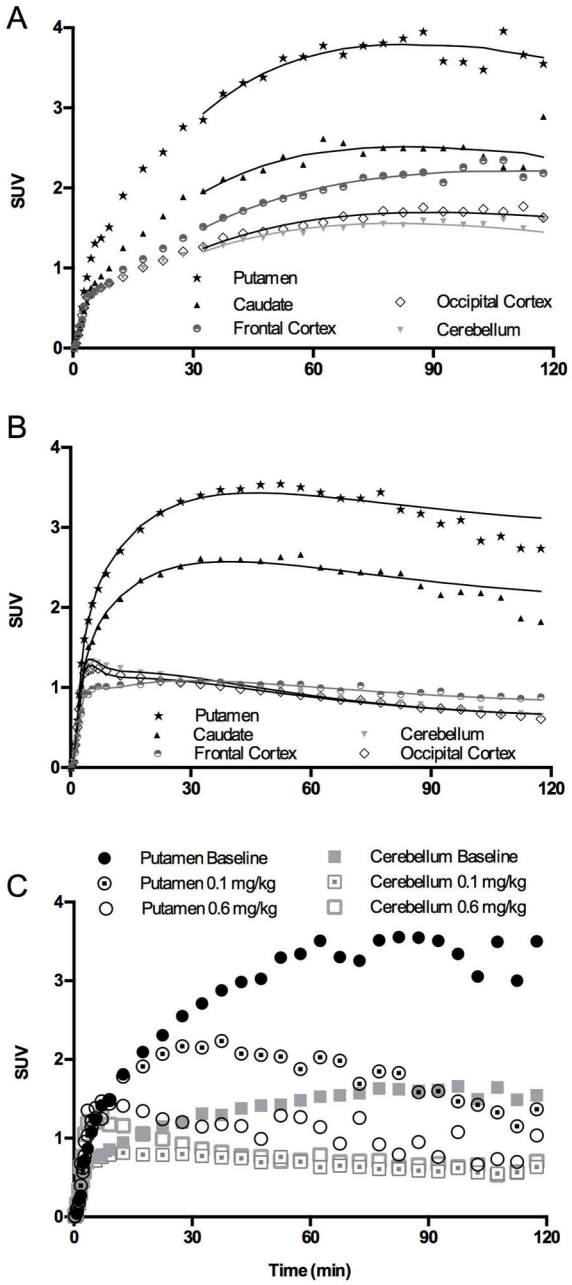


**Figure 3.**

A. [$^{11}$C]MP-10 baseline TACs in the monkey brain with MA1 fits (t* = 30 min). B. [$^{11}$C]MP-10 baseline TACs in the baboon brain with 2T fits from Plisson *et al*. (2011). C. TACs in the putamen and cerebellum of rhesus monkeys pretreated with MP-10 in comparison with the baseline scan. Radioactivity concentrations are expressed as SUV (concentration / (injected dose/body weight)).

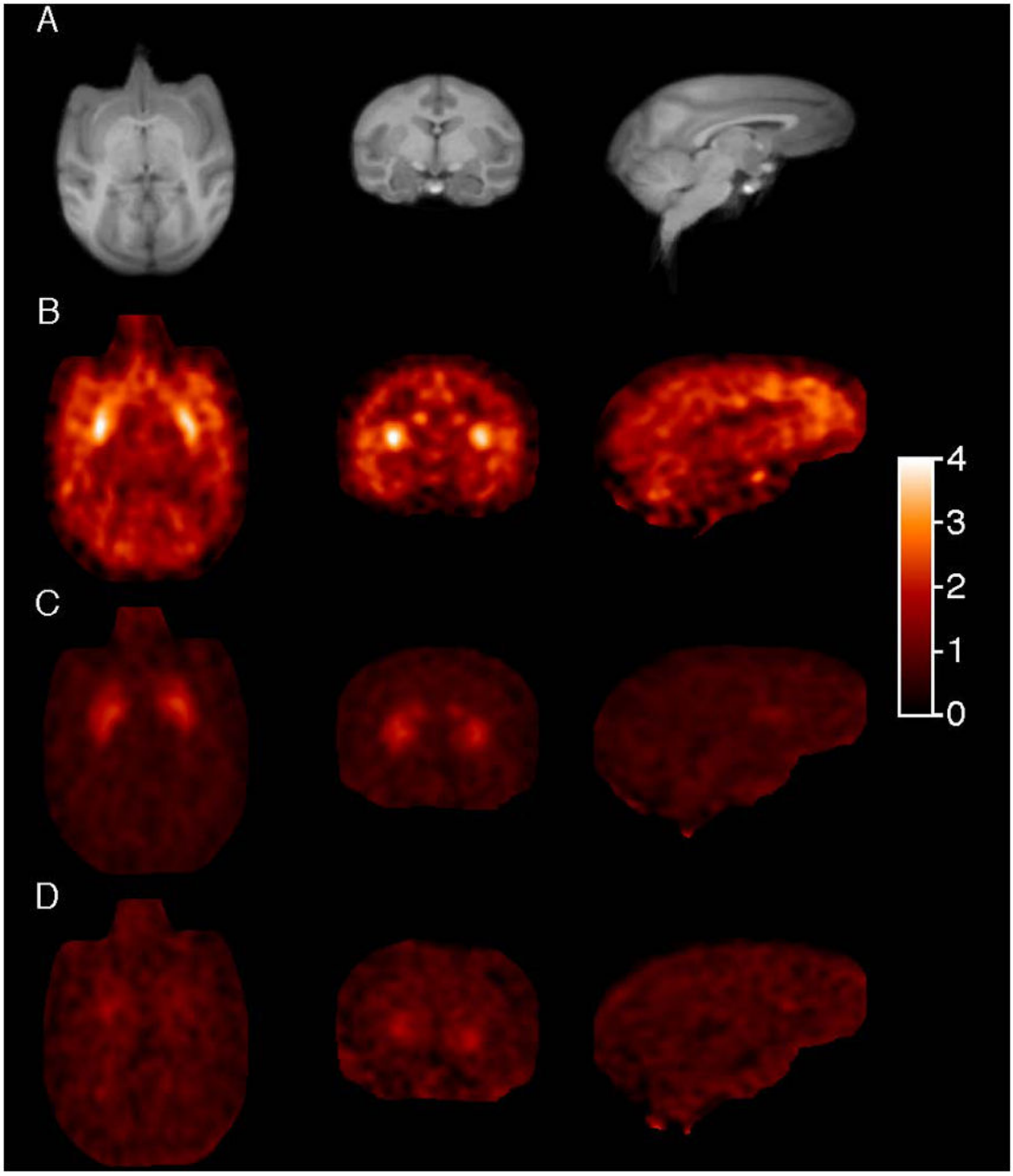


**Figure 4.**

Transverse, coronal and sagittal PET images in rhesus monkey brain summed from 60 to 90 min post-injection of [11C]MP-10 displayed in SUV units [concentration / (injected dose/ body weight)] from a baseline scan (B), and blocking scans with 0.1 mg/kg (C), and 0.6 mg/kg of unlabeled MP-10 (D), together with the corresponding MR images (A).

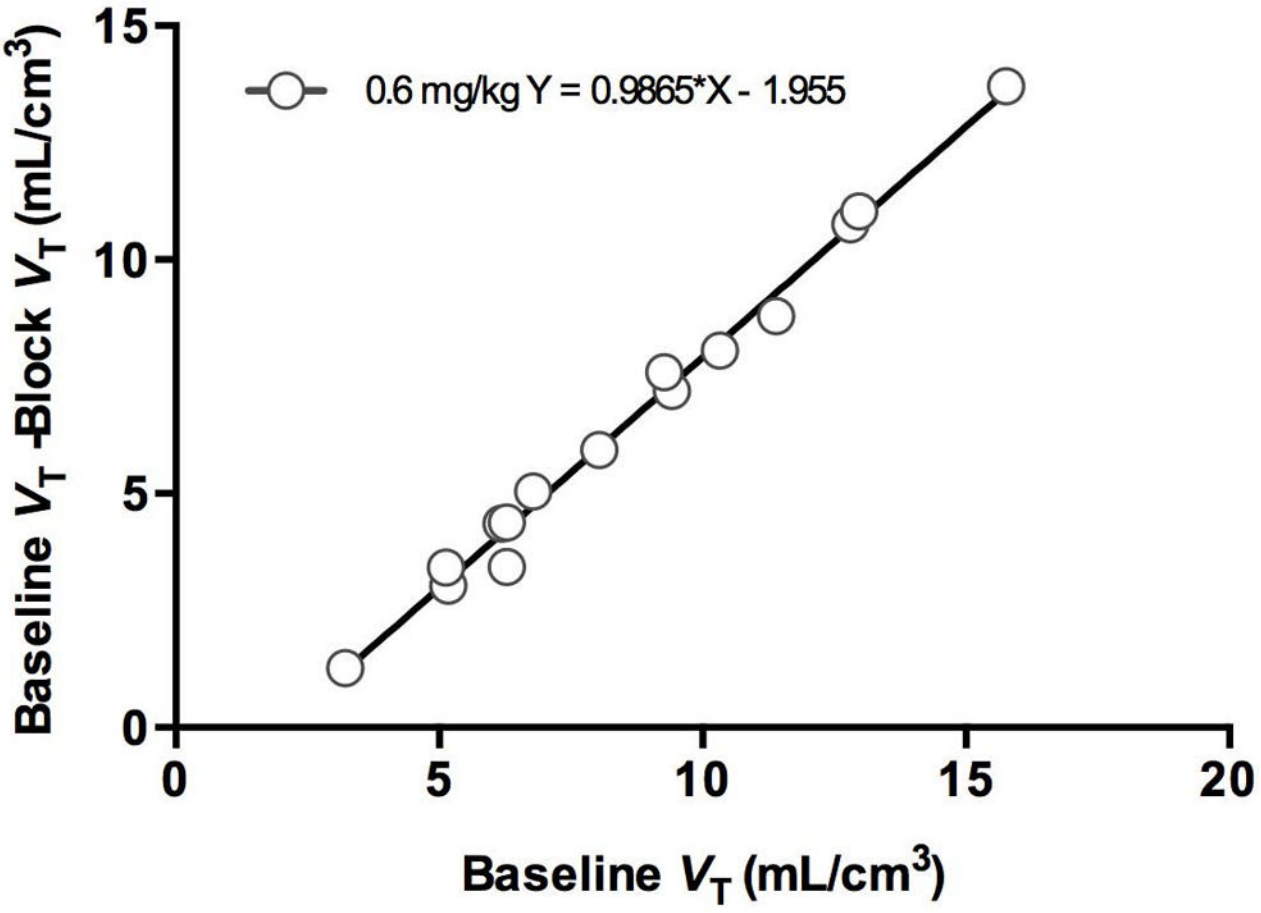


**Figure 5.**
Example occupancy plot for the blocking scan with 0.6 mg/kg of MP-10.

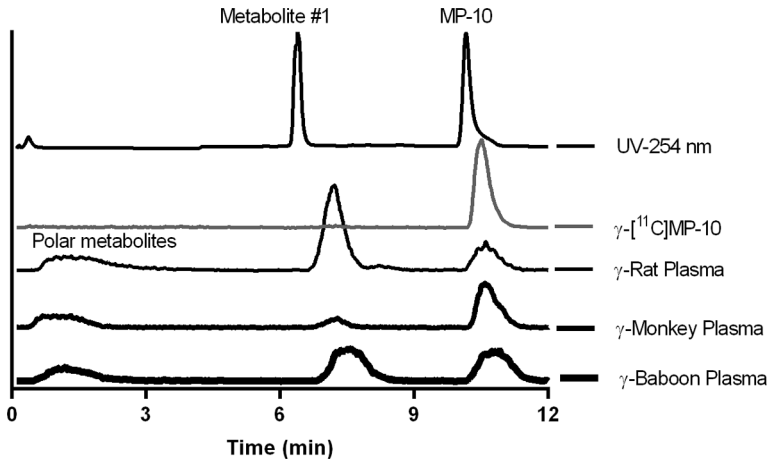


**Figure 6.**

Representative HPLC chromatograms of plasma samples from rat, monkey and baboon at 60 min post-injection of [$^{11}$C]MP-10. Samples were co-injected with authentic, unlabeled metabolite #1 and MP-10.

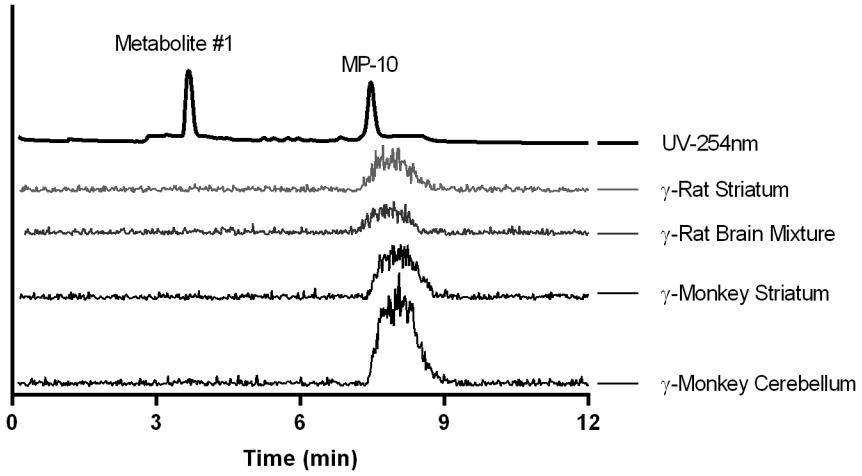


**Figure 7.**

HPLC chromatograms of brain tissue extracts from rat (60 min post-injection) and monkey (45 min post-injection). Samples were co-injected with authentic, unlabeled metabolite #1 and MP-10.

**Table I**

Regional volume of distribution ($V_T$) and $BP_{ND}$* estimates derived from MA1 analysis of baseline and MP-10 blocking scans in 4 different rhesus monkeys.

| ROIs | $V_T$ (mL/cm$^3$) | | $BP_{ND}$ | $V_T$ (mL/cm$^3$) | | $BP_{ND}$ | $V_T$ (mL/cm$^3$) | | $BP_{ND}$ | $V_T$ (mL/cm$^3$) | | $BP_{ND}$ |
|---|---|---|---|---|---|---|---|---|---|---|---|---|
| | Baseline 1 | 0.01 mg/kg | Baseline 1 | Baseline 2 | 0.1 mg/kg | Baseline 2 | Baseline 3 | 0.3 mg/kg | Baseline 3 | Baseline 4 | 0.6 mg/kg | Baseline 4 |
| **Putamen** | 4.8 | 3.3 | *10.1* | 17.2 | 5.8 | *6.7* | 3.4 | 0.9 | *4.5* | 11.4 | 2.6 | *4.8* |
| **Cingulate Cortex** | 4.4 | 2.0 | *9.3* | 18.0 | 2.5 | *7.1* | 5.1 | 0.6 | *7.2* | 12.8 | 2.1 | *5.5* |
| **Frontal Cortex** | 4.3 | 1.9 | *8.9* | 13.6 | 2.6 | *5.1* | 5.6 | 0.7 | *8.1* | 15.8 | 2.1 | *7.0* |
| **Caudate** | 4.3 | 2.6 | *8.9* | 11.2 | 4.5 | *4.0* | 4.2 | 0.7 | *5.8* | 9.4 | 2.2 | *3.8* |
| **Globus Pallidus** | 4.2 | 2.6 | *8.8* | 11.7 | 6.3 | *4.3* | 3.6 | 1.4 | *4.9* | 6.3 | 2.9 | *2.2* |
| **Insula** | 3.9 | 2.0 | *8.1* | 14.4 | 2.3 | *5.4* | 5.2 | 0.5 | *7.4* | 13.0 | 1.9 | *5.5* |
| **Temporal Cortex** | 3.3 | 1.6 | *6.7* | 11.2 | 2.0 | *4.0* | 3.5 | 0.4 | *4.6* | 9.3 | 1.7 | *3.7* |
| **Occipital Cortex** | 2.7 | 1.4 | *5.2* | 8.4 | 2.1 | *2.8* | 2.9 | 0.5 | *3.7* | 6.8 | 1.7 | *2.4* |
| **Thalamus** | 2.3 | 1.6 | *4.4* | 6.8 | 1.9 | *2.0* | 2.4 | 0.5 | *3.0* | 5.1 | 1.7 | *1.6* |
| **Cerebellum** | 2.3 | 1.3 | *4.3* | 6.8 | 2.2 | *2.0* | 2.9 | 0.5 | *3.7* | 6.2 | 1.8 | *2.1* |
| **Brainstem** | 1.8 | 1.2 | *3.2* | 4.4 | 2.4 | *1.0* | 1.7 | 0.5 | *1.7* | 3.2 | 1.9 | *0.6* |

* $BP_{ND}$ values were calculated from individual $V_T$ and $V_{ND}$ values, as $BP_{ND} = (V_{T\ ROI} - V_{ND}) / V_{ND}$; $V_{ND}$ was estimated as the x-intercept of the regression line in the occupancy plot (Figure 5).

**Table II**

The radioactive metabolite profile of monkey brain tissues and plasma of monkeys and baboons

| | Monkey | | | | | Baboon |
|---|---|---|---|---|---|---|
| | Plasma[1] (45 min) | Brain Tissue Extracts[1, 2] | | | Plasma[3] (60 min) | Plasma[3] (60 min) |
| | | Frontal Cortex | Striatum | Cerebellum | | |
| Parent Fraction | 72.3 | 98.8±0.3 | 97.5±2.9 | 97.8±1.4 | 57.9 ±5.0 | 38.7±0.1 |
| Metabolite #1[4] | 6.0 | 1.2±0.3 | 2.5±2.9 | 2.2±1.4 | 9.9±3.6 | 27.6±9.0 |
| Polar metabolites[5] | 21.7 | - | - | - | 32.2±5.9 | 33.7±10.2 |

[1] Plasma and brain samples taken at 45 min after [$^{11}$C]MP-10 injection from one monkey in the *ex vivo* study.

[2] SD calculated from 2 subsamples for each region.

[3] Plasma samples taken at 60 min post-injection from rhesus monkeys (n = 4) and baboons (n = 25) undergoing baseline [$^{11}$C]MP-10 scans.

[4] Retention time of plasma samples with the column-switching HPLC system: ~7.5 min; ~3.5 min for brain tissue extracts in the analytical HPLC system without column-switching.

[5] Radioactivity from the first 4 min of eluent from the column-switching HPLC system.

**Table III**

Metabolite analysis results from rat *ex vivo* study at 30 (n = 2) and 60 min (n = 2) post-injection of [$^{11}$C]MP-10.

| % ± SD | 30 min | | | 60 min | | |
|---|---|---|---|---|---|---|
| | Plasma | Brain Tissue Extracts | | Plasma | Brain Tissue Extracts | |
| | | Striatum | Mixture[1] | | Striatum | Mixture[1] |
| Parent Fraction | 52.4±2.7 | 97.3 | 97.5±0.6 | 32.4±18.8 | 98.0±0.8 | 94.0 |
| Metabolite #1[2] | 31.2±5.4 | 2.7 | 2.5±0.6 | 38.5±11.5 | 2.0±0.8 | 6.0 |
| Polar Metabolites[3] | 16.4±2.7 | - | - | 29.1±7.3 | - | - |

[1] Mixture of frontal cortex, hippocampus, and cerebellum.

[2] Retention time of plasma samples with the column-switching HPLC system: ~7.5 min; ~3.5 min for brain tissue extracts in the analytical HPLC system without column-switching.

[3] Radioactivity from the first 4 min of eluent from the column-switching HPLC system.